Lithos 116 (2010) 145–152

Contents lists available at ScienceDirect

Lithos

journal homepage: www.elsevier.com/locate/lithos

U–Th isotopes in Hainan basalts: Implications for sub-asthenospheric origin of EM2 mantle endmember and the dynamics of melting beneath Hainan Island

Haibo Zou [a,*], Qicheng Fan [b]

[a] Department of Geology and Geography, Auburn University, Auburn, AL 36849, USA
[b] Institute of Geology, China Earthquake Administration, Beijing 100029, China

ARTICLE INFO

Article history:
Received 1 November 2009
Accepted 16 January 2010
Available online 25 January 2010

Keywords:
Basalts
U–Th disequilibrium
Hainan Island
Hotspot
Plume

ABSTRACT

Extensive (about 5000 km^3) basaltic magmas erupted on the Hainan Island, south China, mostly during the past 1 million years. U–Th disequilibrium data as well as Nd, Sr, Pb isotopes and major and trace element concentrations were measured on the youngest lavas from Maanling volcano and Leihuling volcano of the Hainan Island. All the Holocene Hainan basalts display light rare earth element (LREE) enriched patterns and ocean island basalt (OIB)-type incompatible element distributions. Their ε_{Nd} values range from +4.1 to +4.8, $^{87}Sr/^{86}Sr$ ratios vary from 0.7039 to 0.7042, and $^{206}Pb/^{204}Pb$ ratios range from 18.63 to 18.71. The Hainan lavas are characterized by their depleted Sr–Nd isotopic compositions and Dupal-like EM2 (enriched mantle 2) Pb isotope signatures with time-integrated high Th/U and $^{235}U/Pb$.

The olivine tholeiites from Maanling display 18–20% ^{230}Th excesses and the alkali olivine basalts from Leihuling show 22–32% ^{230}Th excesses. The pronounced ^{230}Th excesses in the Holocene basalts indicate that the Holocene Hainan lavas were produced by melting of a mantle source in the garnet stability field (>75 km). Since the lithosphere thickness beneath the Hainan Island is thin (55 km), the garnet peridotite mantle source for the Hainan basalts is not located in the lithospheric mantle. The Nd isotopic compositions do not indicate a highly depleted asthenospheric mantle source. We thus suggest that the EM2 mantle source for the young Hainan basalts is in the mantle transition zone or more likely lower mantle, which is consistent with a plume origin. The significant ^{230}Th excesses also suggest slow (<1 cm/year) upwelling, possibly indicative of a weakly buoyant mantle plume. The older EM2 Cenozoic basalts from Hainan, South China Sea Basin and adjacent areas may also originate from partial melting of lower mantle materials in the rising Hainan plume.

1. Introduction

The volcanic eruptions in the northern Hainan Island (20°N, 110°E), south China, produced about 5000 km^3 basaltic magmas (Fig. 1). Although the eruptions may have initiated more than 1 million years ago, most of the basalts were produced over a time interval of 200,000 to 500,000 years (Flower et al., 1992). The average magma supply of 0.1 to 0.25 km^3/year approaches that of a major flood basalt episode (Flower et al., 1992). The Hainan eruptions are part of a regional magmatic episode surrounding the South China Sea Basin and nearby regions, such as Vietnam (Hoang and Flower, 1998), Thailand (Zhou and Mukasa, 1997) and SE China (Zou et al., 2000). These volcanic rocks surrounding the South China Sea Basin, and those from seamounts within the South China Sea Basin, are younger than the South China Sea sea-floor extension, i.e., postdating the opening of the South China Sea Basin (at 30 to 16 million years ago).

The Hainan lavas, located at the northern edge of the South China Sea Basin, may present a microcosm of the volcanic activity surrounding the South China Sea Basin (Flower et al., 1992). It has been recognized (Tu et al., 1991; Flower et al., 1992) that (1) chemically the Hainan basalts resemble the oceanic island basalts (OIB) with enriched OIB-type incompatible element distributions, and (2) isotopically the Hainan basalts are characterized by the intriguing Dupal-like Pb isotopic signatures and depleted Sr–Nd isotopic compositions. There are still debates about the origins of the Hainan volcanoes, with implications for the origins of the 'Southern Hemisphere' Dupal anomaly in the Northern Hemisphere Hainan basalts (Tu et al., 1991; Tu et al., 1992; Liu, 1999; Zhao, 2007). On a global scale, it is not clear whether such Dupal mantle reservoirs are mainly derived from shallow subcontinental lithospheric mantle (Hawkesworth et al., 1990; Tu et al., 1991) or from deep mantle (e.g., lower mantle) (Hart, 1984; Castillo, 1988; Hart et al., 1992).

To provide new insights into the origins of the Hainan basalts, additional geological tools (in addition to Nd, Sr and Pb isotopes and seismic images) are needed. Young basalts erupted ~9000 years (9 ka) ago at Maanling volcano and Leihuling volcano (Fan et al., 2004) in

* Corresponding author. Tel.: +1 334 844 4315; fax: +1 334 844 4486.
E-mail addresses: haibo.zou@gmail.com, haibo.zou@auburn.edu (H. Zou).

0024-4937/$ – see front matter © 2010 Elsevier B.V. All rights reserved.
doi:10.1016/j.lithos.2010.01.010

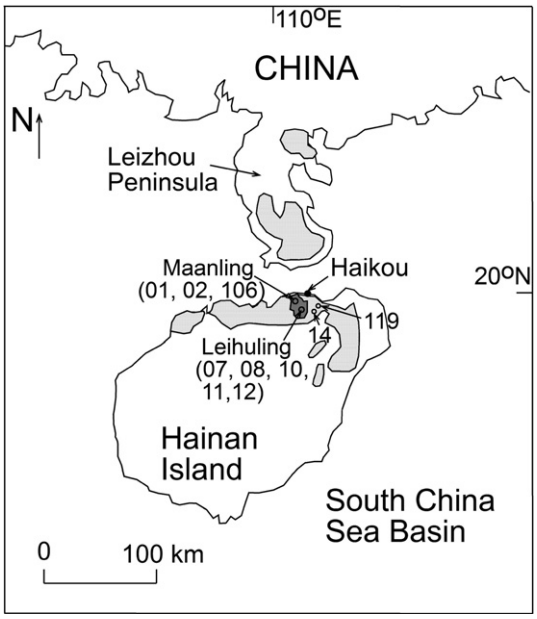

Fig. 1. Distribution of late Cenozoic basalts in the northern Hainan Island and Leizhou Peninsula, and sample locations. Shaded areas are late Cenozoic basalts. The dark shaded area represents locations of Holocene lavas.

Hainan Island. These young basalts provide ideal opportunities to apply short-lived U–Th disequilibrium to investigate the origins of the Hainan basalts. U–Th disequilibrium has been demonstrated as an effective tool for investigating the origins of young basalts (Asmerom and Edwards, 1995; Reid, 1995; Asmerom, 1999). Although EM2-like Cenozoic basalts are widespread in the South China Sea Basin and nearby regions, such as Vietnam (Hoang and Flower, 1998) and Thailand (Zhou and Mukasa, 1997) and SE China (Zou et al., 2000), few basalts are young enough for the short-lived U–Th disequilibrium studies.

Here we carry out a systematic U–Th disequilibrium, Nd, Sr and Pb isotope as well as major and trace element study of young lavas from Hainan Island. Our aims are (1) investigate the origins of the Hainan Holocene lavas and the possible link with plume volcanism and (2) constrain the melting conditions below Hainan Island. Obviously this U–Th disequilibrium study builds on pioneering Nd–Sr–Pb isotope studies of the Hainan basalts (Tu et al., 1991; Flower et al., 1992) and recent seismic tomographic imaging (Lebedev and Nolet, 2003; Huang and Zhao, 2006; Lei and Zhao, 2009).

2. Analytical methods

Thorium isotopic compositions of most samples were measured using a VG 54 mass spectrometer equipped with a WARP energy filter (VG54-WARP) and an ion counting system, except for 3 samples (HN106, HN119 and HN11) that were measured by a Cameca IMS 1270 ion microprobe at UCLA. The mass resolution for the ion probe IMS 1270 work is at 5000. The revised chemical method (Zou et al., 2008) to separate and purify thorium involves two columns (1) a 400 μl TRU Spec column to separate Th from other major and trace elements, and (2) a 100 μl anion resin column to purify Th. Major and trace elements were measured by ICP-MS at the GeoAnalytical Center at the Washington State University and the Institute of Geology and Geophysics, Chinese Academy of Sciences. Sample powders were prepared with an agate mill. Nd, Sr and Pb isotopic compositions as well as U and Th concentrations were measured using VG 54 WARP at UCLA. Analytical details on Nd, Sr and Pb isotopes and U and Th concentrations at UCLA using TIMS have been documented in Zou et al. (2003). Nd and Sr isotopic compositions were normalized to $^{146}Nd/^{144}Nd = 0.7219$ and $^{86}Sr/^{88}Sr = 0.1194$, respectively. The measured Nd and Sr isotope standard values are $^{143}Nd/^{144}Nd = 0.511843 \pm 13$ ($n = 24$) for La Jolla and $^{87}Sr/^{86}Sr = 0.710239 \pm 16$ ($n = 13$) for NBS 987. Replicate analyses of Pb isotope standard NBS 981 give $^{206}Pb/^{204}Pb = 16.896 \pm 0.013$, $^{207}Pb/^{204}Pb = 15.435 \pm 0.014$, and $^{208}Pb/^{204}Pb = 36.525 \pm 0.041$. Relative to the following values for NBS981: $^{206}Pb/^{204}Pb = 16.9356$, $^{207}Pb/^{204}Pb = 15.4891$, and $^{208}Pb/^{204}Pb = 36.7006$ (Todt et al., 1996), Pb isotopic data in samples were corrected for mass fractionation of 0.118% per atomic mass unit (AMU) for $^{206}Pb/^{204}Pb$, 0.117% per AMU for $^{207}Pb/^{204}Pb$, and 0.119% per AMU for $^{208}Pb/^{204}Pb$.

3. Results

We selected 10 samples for major, trace element and isotope analyses, including 3 Holocene samples from Maanling, 5 Holocene samples from Leihuling and 2 Pleistocene samples from Sanjiaoyuan (HN14) and Bopian (HN119) (Fig. 1). Major and trace element concentrations (in wt.%) are presented in Table 1. According to CIPW norms (Table 1), the Maanling samples are olivine tholeiites, and the Leihuling samples are mostly alkali olivine basalts with minor olivine tholeiites. As for the two older Pleistocene rocks, the Sanjiaoyuan sample (HN14) is olivine tholeiite and the Bopian sample (HN119) is quartz tholeiite.

The MgO content varies from 6.5% to 7.5% for Maanling tholeiites, and 9.6% to 12.8% for Leihuling alkali basalts, 9.1% for Sanjiaoyuan and 6.8% for Bopian. Their mg numbers (molar $Mg/(Mg + Fe^{2+})$) are 0.59 to 0.61 for Maanling, 0.65–0.66 for Leihuling, 0.67 for Sanjiaoyuan and 0.61 for Bopian. The Holocene basalts from Leihuling and Maanling have high TiO_2 contents, ranging from 2.3 to 2.8%. The Pleistocene lavas have lower TiO_2 (2.2–1.6%).

All basaltic rocks from Hainan Island are enriched in light rare earth elements (LREEs) over heavy rare earth elements (HREEs) (Fig. 2). None of the samples displays any negative Eu anomalies. In the spider diagram (Fig. 2), except for HN119, all samples show appreciable enrichment in high field strength elements (HFSEs), such as Nb and Ta.

The Sr, Nd and Pb isotope data show highly restricted range within each locality (Table 2). The ε_{Nd} values are +4.5 to +4.8 for Maanling, and +4.1 to +4.4 for Leihuling. The $^{87}Sr/^{86}Sr$ values range from 0.70385 to 0.70392 for Maanling, and 0.70418 to 0.70427 for Leihuling. The $^{206}Pb/^{204}Pb$ ratios are 18.10 to 18.63 for Maanling, and 18.66 to 18.70 for Leihuling.

The Nd isotope compositions indicate that source rocks for the Maanling and Leihuling lavas are moderately depleted and are homogeneous. The Hainan basalts are less depleted as compared to the Central Indian Ridge MORBS or some basalts from central East China (Fig. 3). In the $^{207}Pb/^{204}Pb$ vs. $^{206}Pb/^{204}Pb$ and $^{208}Pb/^{204}Pb$ vs. $^{206}Pb/^{204}Pb$ diagrams (Fig. 4), all samples plot above the Northern Hemisphere Reference Line (NHRL) (Hart, 1984) and thus display Dupal Pb anomalies (Tu et al., 1991; Flower et al., 1992). The Nd–Sr–Pb isotope data suggest that they are EM2 like basalts (Figs. 3 and 4).

The U–Th isotope results are presented on a ($^{230}Th/^{232}Th$) vs. ($^{238}U/^{232}Th$) equiline diagram in Fig. 5. All Holocene samples (Maanling and Leihuling) display significant ^{230}Th excesses (Fig. 5). The ($^{230}Th/^{238}U$) values are 1.18 to 1.20 for Maanling, and 1.23 to 1.32 for Leihuling. One Pleistocene basaltic sample (HN14) has ($^{230}Th/^{238}U$) value of 1.10 and another Pleistocene quartz tholeiite displays U–Th equilibrium.

4. Discussion

The Hainan samples appear to be relatively primitive basalts without significant crustal contamination or fractional crystallization. All the samples have high mg numbers (0.59 to 0.67) (Table 1). Their high mg numbers suggest that the samples closely reflect source compositions and mantle processes, and are not significantly affected

Table 1
Major element (in wt.%) and trace element (ppm) concentrations of Hainan basalts.

Sample	HN9901	HN9902	106B1	HN9907	HN9907*	HN9908	HN9910	HN9911	HN9912	HN9912*	HN9914	119B1
	OT	OT	OT	OT		AOB	AOB	AOB	AOB		OT	QT
Locality	Maanling	Maanling	Maanling	Leihuling		Leihuling	Leihuling	Leihuling	Leihuling		Sanjiaoyuan	Bopian
SiO_2	51.74	50.77	50.99	49.10		45.32	45.47	45.14	45.27		49.87	53.14
TiO_2	2.34	2.37	2.27	2.30		2.81	2.76	2.76	2.75		2.17	1.62
Al_2O_3	14.32	15.12	14.33	13.36		12.83	12.98	12.99	12.76		13.86	14.36
Fe_2O_3*	10.64	10.42	10.97	11.42		12.79	12.67	11.52	12.63		10.41	10.07
MnO	0.15	0.25	0.14	0.27		0.20	0.31	0.19	0.20		0.15	0.14
MgO	6.53	6.81	7.47	9.63		10.29	10.17	9.90	10.29		9.08	6.80
CaO	8.92	9.24	9.28	9.46		10.57	10.80	10.43	10.46		9.37	8.53
Na_2O	3.41	2.82	2.71	2.55		2.85	2.42	2.95	3.12		3.12	3.03
K_2O	1.68	1.46	1.38	1.53		1.64	1.43	1.61	1.63		1.53	1.00
P_2O_5	0.47	0.47	0.47	0.48		0.86	0.82	0.75	0.79		0.42	0.23
Total	100.19	99.73	100.02	100.11		100.15	99.84	98.24	99.88		99.97	98.93
mg#	0.59	0.60	0.61	0.66		0.65	0.65	0.66	0.65		0.67	0.61
CIPW												
Quartz	0	0	0	0		0	0	0	0		0	2.55
Plagioclase	48.01	48.73	46.19	42.47		30.06	35.58	31.64	27.99		46.14	49.24
Orthoclase	9.99	8.75	8.27	9.1		9.81	8.57	9.81	9.75		9.1	6.03
Nepheline	0	0	0	0		6.41	3.11	6.49	8.1		0	0
Diopside	18.43	15.27	16.52	19.02		24.11	22.93	24.45	25.29		20	15.17
Hypersthene	10.04	17.51	19.74	7.24		0	0	0	0		1.01	21.85
Olivine	6.4	2.57	2.2	14.95		20.35	20.7	18.72	19.9		17.07	0
Ilmenite	4.48	4.56	4.35	4.43		5.37	5.32	5.39	5.28		4.16	3.13
Magnetite	1.55	1.52	1.61	1.67		1.87	1.86	1.73	1.86		1.52	1.49
Apatite	1.09	1.09	1.11	1.14		2.02	1.92	1.78	1.83		0.97	0.56
Cs	0.57	0.61	nd	0.42	0.40	0.46	0.71	0.82	0.71	0.71	0.39	0.52
Rb	35.6	30.0	28.8	32.4	32.41	36.5	35.0	35.2	38.8	39.0	30.0	23.6
Ba	396	423	351	396	396	573	574	535	536	541	353	216
Th	3.87	3.90	4.29	4.70	4.13	8.36	8.29	7.63	7.76	6.71	3.38	2.73
U	0.91	0.88	0.99	1.19	1.02	2.00	1.96	1.81	1.81	1.54	0.79	0.59
Nb	33.61	33.70	41.06	46.11	51.09	84.08	83.90	77.05	79.05	86.71	33.78	16.40
Ta	2.04	2.04	2.44	2.80	3.51	5.20	5.25	4.77	4.79	5.61	2.05	0.98
La	24.93	24.94	29.52	33.26	35.91	64.82	64.09	58.88	59.40	63.74	22.30	14.02
Ce	49.4	49.6	57.6	65.2	66.3	125.7	125.5	114.8	116.5	117.1	43.4	27.5
Pb	3.03	3.53	4.06	3.53	3.39	5.19	5.27	3.98	4.84	4.91	2.48	2.79
Pr	6.20	6.26	7.38	7.83	7.87	14.79	14.71	13.55	13.58	13.56	5.40	3.44
Sr	546	559	489	557	583	817	820	769	811	843	525	318
Nd	26.9	27.1	30.8	32.0	31.31	57.2	57.0	52.3	52.2	51.56	23.0	15.2
Zr	188	189	198	191	195	309	309	289	294	302	152	108
Hf	4.85	4.92	4.80	4.87	4.72	7.60	7.72	7.24	7.16	6.92	3.93	3.02
Sm	6.94	6.83	6.64	7.07	6.78	10.89	10.77	10.26	10.10	9.95	5.79	4.14
Eu	2.34	2.36	2.11	2.33	2.10	3.35	3.37	3.15	3.24	2.87	2.05	1.48
Gd	6.79	6.85	6.44	6.52	6.18	9.12	9.15	8.85	8.65	8.19	5.95	4.56
Tb	1.03	1.01	0.96	0.97	0.87	1.28	1.29	1.24	1.23	1.12	0.88	0.73
Dy	5.52	5.51	5.22	5.25	4.61	6.96	6.94	6.65	6.53	5.89	4.87	4.18
Ho	0.98	0.96	0.91	0.94	0.82	1.23	1.21	1.18	1.16	1.02	0.86	0.78
Er	2.26	2.20	2.19	2.23	2.08	2.97	2.87	2.77	2.72	2.54	2.07	1.89
Yb	1.61	1.53	1.78	1.66	1.61	2.17	2.15	2.04	2.06	2.03	1.46	1.44
Y	23.4	23.3	25.5	22.7	24.4	30.0	29.8	28.6	29.1	31.0	21.2	18.8
Lu	0.22	0.22	0.26	0.24	0.24	0.32	0.32	0.30	0.31	0.31	0.22	0.21
Eu*	1.03	1.05	0.97	1.03	0.97	1.00	1.01	0.99	1.03	0.94	1.06	1.04
Sr/Th	141	143	114	119	141	98	99	101	105	126	155	117
Ba/Th	103	108	82	84	96	69	69	70	69	81	104	79

Eu anomaly is given by $Eu^* = 2Eu_N/(Sm_N + Gd_N)$, where *N* denotes normalized values by CI chondrite.
OT = olivine tholeiite; AOB = alkali olivine basalt; QT = quartz tholeiite. HN9907* and HN9912* are duplicates. mg# = mg/(Mg + Fe^{2+}), assuming $Fe^{3+}/Fe^{2+} = 0.15$.
Fe_2O_3*: total iron as Fe_2O_3.

by continental contamination during magma ascent. In addition, strong ^{230}Th excesses in Hainan basalts cannot be produced from crustal contaminations because bulk assimilation of crustal rocks with (^{230}Th/^{238}U) = 1.0 can only reduce the extent of ^{230}Th excesses.

4.1. Evidence against subduction-related fluid-induced melting

Our U–Th disequilibrium data, together with trace element data, do not indicate possible influence of subduction-related fluids in the mantle. Uranium is highly mobile in oxidizing aqueous fluids whereas thorium behaves as an immobile HFSE. The subduction-related fluids are thus highly enriched in U relative to Th. Lavas formed by recent subduction-related fluid-induced melting often display ^{238}U excesses or U–Th equilibrium (Gill and Williams, 1990; Elliott et al., 1997; Turner et al., 2003), whereas the Hainan lavas display significant ^{230}Th excesses. High field strength elements such as Nb and Ta behave similarly to the immobile Th during slab dehydration. The typical fluid-induced melting along magmatic arcs generates lavas with negative anomalies in Nb and Ta (e.g., Gill, 1981; Elliott, 2003). Hainan basalts display positive Nb and Ta anomalies (Fig. 2), which do not indicate the involvement of recent subduction-related fluids or sediments.

To sum up, the significant ^{230}Th excesses and the positive anomalies in Nb and Ta, consistently argue against the involvement of subduction-related fluids to generate the Hainan lavas.

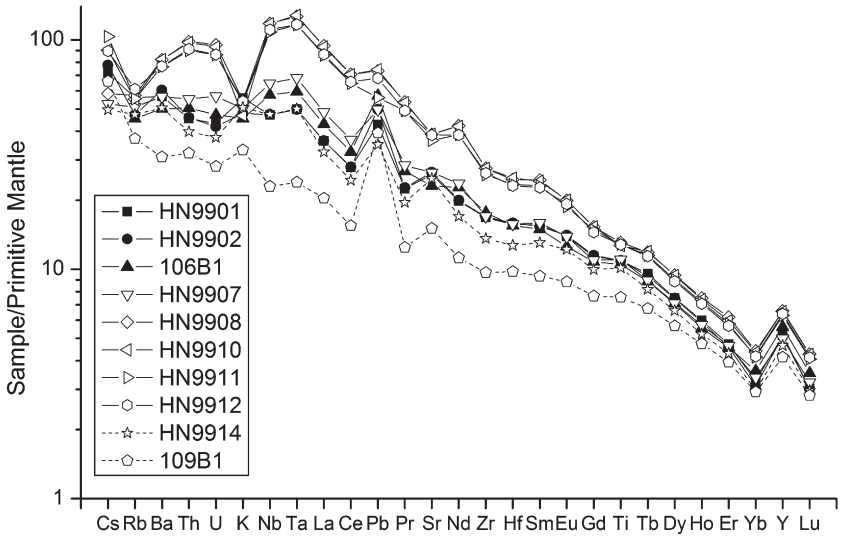

Fig. 2. Primitive mantle normalized trace element diagrams for Hainan lavas. Note positive Nb and Ta anomalies and steep REE patterns for the Holocene basalts. Sun and McDonough, 1989.

4.2. Depth and location of melting: evidence for plume melting

After ruling out the possibility of fluid-induced melting, we suggest that decompressional melting is the most likely mechanism to generate the Hainan basalts. An important question regarding decompressional melting is the depth and location of melting, which is critical for understanding the origin of the Hainan basalts.

The significant (18–32%) ^{230}Th excesses in all samples from Maanling and Leihuling require mantle melting in the garnet stability field. This is due to the fact that garnet is the dominant mineral phase in the mantle where thorium is significantly more incompatible than uranium during mantle melting (Beattie, 1993; LaTourrette et al., 1993; Salters and Longhi, 1999). The steep REE patterns (Fig. 2) also indicate that garnet is a residual phase during mantle melting, in addition to the initial REE patterns of the source. In comparison, U–Th disequilibrium in basalts is independent of source composition as long as the source is in secular equilibrium ((^{230}Th/^{238}U) = 1) prior to melting. The secular equilibrium in the mantle prior to melting can be easily achieved in 0.35 million years (i.e., five half lives of ^{230}Th). Thus the significant ^{230}Th excesses in the young Hainan basalts significantly strengthen the argument of garnet involvement. Because the pressure for the spinel peridotite to garnet peridotite transition in the mantle is at 75 km, melting beneath Hainan Island took place at the depth of >75 km.

Garnet signature from U–Th disequilibrium may not be exclusively limited to garnet peridotite, as garnet pyroxenites (with olivine content ranging from 0 to 40%) also contains garnet. Although tholeiites cannot be generated by garnet pyroxenites, it has been demonstrated that alkali basalts can be generated by melting of silica-poor garnet pyroxenite (Hirschmann et al., 2003). However, alkali basalts produced by melting of garnet pyroxenite at low pressure (1–2 Gpa) have consistently higher Al_2O_3 (15.2 to 16.2%) (Hirschmann et al., 2003) as compared to Hainan (12–13%; Table 1) alkali basalts. To generate alkali basalts with Al_2O_3 similar to Hainan alkali basalts (12–13%) (Table 1), melting of garnet pyroxenite has to take place at high pressure (5 Gpa, or 165 km) (Kogiso et al., 2003). Thus the significant ^{230}Th excess in the Hainan lavas require deep (>75 km) melting, and even deeper if the source is garnet pyroxenite.

The lithosphere beneath the Hainan Island is relatively thin (55 km) (Wu et al., 2004). The identification of deep melting in the garnet stability field by U–Th disequilibrium indicates that the Hainan basalts were generated below the base of the subcontinental lithosphere at Hainan.

Possible deep mantle sources below the base of mantle lithosphere include the asthenosphere, transition zone and lower mantle. Since the Nd isotopic compositions of the Hainan lavas are significantly lower than the asthenospheric values represented by the Central

Table 2
U–Th disequilibrium and Nd, Sr and Pb isotopic compositions.

Samples	HN01	HN02	HN106	HN07	HN08	HN10	HN11	HN12	HN14	HN119
	OT	OT	OT	OT	AOB	AOB	AOB	AOB	OT	QT
Locations	Maanling	Maanling	Maanling	Leihuling	Leihuling	Leihuling	Leihuling	Leihuling	Sanjiaoyuan	Bopian
U	0.876	0.855	0.906	1.15	1.89	3.18	1.72	1.72	0.739	0.552
Th	3.58	3.54	3.77	4.44	7.81	12.30	7.07	7.18	3.04	2.29
U/Th	0.245	0.241	0.240	0.260	0.242	0.258	0.244	0.240	0.243	0.241
(^{238}U/^{232}Th)	0.744	0.733	0.731	0.789	0.736	0.785	0.740	0.729	0.737	0.734
(^{230}Th/^{232}Th)	0.895	0.870	0.863	0.968	0.936	0.979	0.961	0.962	0.810	0.736
(^{230}Th/^{238}U)	1.203	1.186	1.181	1.227	1.272	1.246	1.299	1.321	1.099	1.003
^{87}Sr/^{86}Sr	0.703853	0.703919		0.704180	0.704230	0.704273		0.704182		
2SE	0.000011	0.000009		0.000015	0.000014	0.000011		0.000013		
^{143}Nd/^{144}Nd	0.512868	0.512884		0.512848	0.512869	0.512861		0.512862		
2SE	0.000010	0.000008		0.000009	0.000008	0.000010		0.000008		
ε_{Nd}	4.5	4.8		4.1	4.5	4.4		4.4		
^{208}Pb/^{204}Pb	38.846			38.874	38.881	38.872		38.853		
^{207}Pb/^{204}Pb	15.605			15.633	15.647	15.630		15.622		
^{206}Pb/^{204}Pb	18.631			18.655	18.692	18.696		18.705		

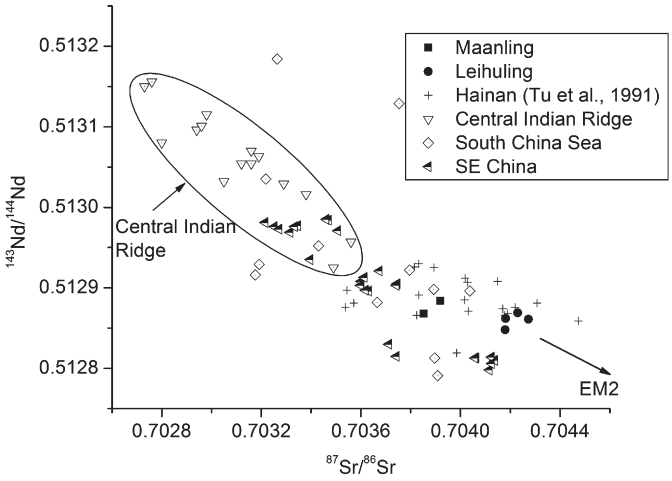

Fig. 3. $^{143}Nd/^{144}Nd$ vs. $^{87}Sr/^{86}Sr$ diagram for Hainan lavas. Data sources: Central Indian Ridge (CIR) (Mahoney et al., 1989); South China Sea (Flower et al., 1992; Tu et al., 1992); previous Hainan data (Tu et al., 1991); and SE China (Zou et al., 2000). Arrow pointing to EM2 composition (Zindler and Hart, 1986).

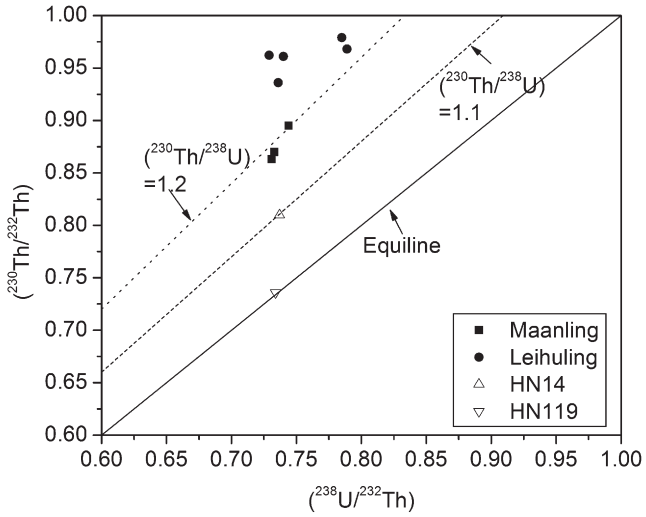

Fig. 5. U–Th disequilibrium data for Hainan lavas.

Indian Ridge MORB or some basalts from central east China (Fig. 3), we suggest that asthenosphere may not be the main source. The mantle source for the Hainan basalts may come from regions below the asthenosphere, such as the transition zone or the lower mantle. This conclusion is made possible owing to the thin lithosphere beneath Hainan and the presence of significant ^{230}Th excesses and moderately depleted Nd isotopic compositions in the Holocene basalts erupted at Maanling and Leihuling on this Island.

The thin lithosphere beneath Hainan Island provides suitable initial conditions for substantial decompressional melting of rising plume materials. It has been demonstrated that thick and cold lithosphere (in cratons, such as Wyoming craton above Yellowstone hotspot) may hinder decompressional melting of rising plume materials (Manea et al., 2009). If a typical craton lithosphere is initially more than 200 km thick, then thinning by at least a factor of two is required to allow decompressional melting of rising plume materials. If lithospheric thinning is insufficient, the lithospheric lid hinders substantial melting of plume materials. Under this condition of still thick lithosphere, substantial melting of the lithospheric mantle occurs, which is the case for Yellowstone hotspot (Leeman et al., 2009; Manea et al., 2009).

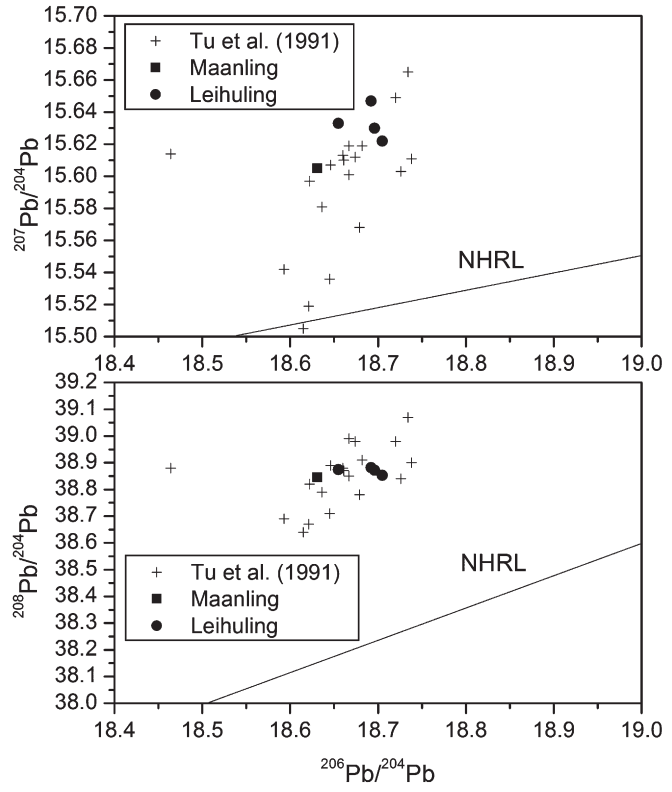

Fig. 4. (a) $^{207}Pb/^{204}Pb$ vs. $^{206}Pb/^{204}Pb$ diagram, and (b) $^{208}Pb/^{204}Pb$ vs. $^{206}Pb/^{204}Pb$ diagram for the lavas from Hainan Island. All data plot above the Northern Hemisphere Reference Line (NHRL) (Hart, 1984). EM2 composition (Zindler and Hart, 1986).

Origins of the Hainan lavas from the transition zone or lower mantle indicated by U–Th disequilibrium and Nd isotopes are consistent with the model of plume melting beneath the Hainan Island (Zhao, 2007). It was previously proposed that the Hainan volcano in south China is a manifestation of a hotspot (Liu, 1999). Recent support for the hypothesis of a plume below Hainan comes from geophysical observations. A high-resolution seismic tomography (Huang and Zhao, 2006) and a waveform tomography (Lebedev and Nolet, 2003) revealed prominent low-velocity anomalies in the upper and lower mantle, down to 1300-km depth under Hainan. On a global scale, Hainan plume is regarded as one of the 12 deep plumes (including Hawaii, Tahiti, Louisville, Iceland, Cape Verde, Reunion, Kerguelen, Amsterdam, Afar, Eifel, Hainan, and Cobb hotspots) with visible continuous low-velocity (low-V) anomalies in both the upper and lower mantle. These deep plumes may be whole-mantle plumes originating from the core–mantle boundary (CMB) (Zhao, 2004; Zhao, 2007).

4.3. Melting conditions

Although U–Th disequilibrium in basalts cannot provide quantitative estimate of maximum depth of melting, it can provide new insight into the rate of melting that is related to the plume upwelling rate. Fast plume upwelling (e.g., Hawaii) can generate basalts with small (a few percent) ^{230}Th excesses, whereas slow plume upwelling (e.g., Iceland) can generate basalts with significant ^{230}Th excesses.

4.3.1. U–Th disequilibrium and rate and degree of melting

In the case of fast plume upwelling and thus high melting rate, ^{230}Th behaves like a long-lived isotope ^{232}Th or a stable element during fast partial melting. $(^{230}Th/^{238}U)$ in the melt produced by fast partial melting is mostly controlled by U–Th elemental fractionation. The elemental fractionation is very limited for highly incompatible

elements U and Th. During dynamic partial melting, the concentration of a trace element in the magma is (Zou, 1998)

$$C_{melt} = \frac{C_0}{X}\left[1-(1-X)^{1/[\Phi + (1-\Phi)D_0]}\right] \quad (1)$$

where C_0 is the source concentration, X is the fraction of extracted melt (or can be regarded as effective degree of melting), Φ is the critical mantle mass porosity, and D_0 is the bulk partition coefficient. The Th/U ratio in the melt is thus related to the Th/U ratio in the source by

$$\frac{Th_{melt}}{U_{melt}} = \frac{Th_0}{U_0} \times \frac{1-(1-X)^{1/[\Phi + (1-\Phi)D_0^{Th}]}}{1-(1-X)^{1/[\Phi + (1-\Phi)D_0^{U}]}} \quad (2)$$

For practical values $D_{Th}=0.003$ and $D_U=0.005$ and $\Phi=0.4\%$, we have $(Th/U)_{melt}=1.11(Th/U)_0$ when $X=1\%$, $(Th/U)_{melt}=1.04(Th/U)_0$ when $X=1.5\%$, and $(Th/U)_{melt}=1.02(Th/U)_0$ when $X=2\%$.

Thus Th/U elemental fractionation factor

$$\delta_{Th/U} = \left(\frac{Th_{melt}}{U_{melt}} \Big/ \frac{Th_0}{U_0}\right)-1 \quad (3)$$

is 11% when $X=1\%$, 4% when $X=1.5\%$, and 2% when $X=2\%$. Note that the fractionation factor δ does not change even if Φ varies in a range of 0.1% to 1%.

The calculation here also indicate that low degree partial melting (1–2%) can generate some ^{230}Th excesses (2–10%) but not significant ^{230}Th excesses (30%). In addition, 1–2% partial melting is usually too low for basalts. The degrees of partial melting are usually 2–5% for alkali basalts and 8–11% for tholeiites (Frey et al., 1978; Zou and Zindler, 1996).

It has been mentioned in a hallmark paper (Williams and Gill, 1989) that low degree (5%) of partial melting is capable of generating significant ^{230}Th excesses. However, the partition coefficients ($D_U=0.015$ and $D_{Th}=0.005$) and D_U/D_{Th} ratio of 3 assumed in their calculation are too high for mantle melting, resulting in higher Th/U fractionation. Experimental results on U and Th partitioning during mantle melting (Beattie, 1993; LaTourrette et al., 1993; Salters and Longhi, 1999) became available only after the publication of their theoretical paper.

In the case of slow melting conditions, ^{230}Th also has time to grow in the mantle owing to the decay of ^{238}U. These newly produced ^{230}Th can also be preferentially partitioned into the melt during slow melting, resulting in higher (^{230}Th/^{238}U) in the melt. Another way to visualize this is to think that ^{230}Th in the melt has an additional supply from ^{238}U decay in the mantle. Note that the slow melting increases the (^{230}Th/^{238}U), but does not influence (^{232}Th/^{238}U) or Th/U elemental ratio, because ^{232}Th (unlike ^{230}Th) has no additional supply.

In summary, both U–Th elemental fractionation and ingrowth contribute to the ^{238}U–^{230}Th disequilibrium in magmas. However, due to the small magnitude of the U–Th elemental fractionation, dominant contributions from the ingrowth of ^{230}Th in the mantle during slow melting is needed in order to produce significant ^{230}Th excess.

4.3.2. Upwelling rate for Hainan plume

Ideally, melting rate and mantle porosity can be constrained using (^{230}Th/^{238}U) and (^{226}Ra/^{230}Th) in young basalts (e.g., Chabaux and Allegre, 1994; Sims et al., 1999; Pietruszka et al., 2001). (^{230}Th/^{238}U) produced by decompression melting is more sensitive to the rate of melting and (^{226}Ra/^{230}Th) is more sensitive to the porosity in the melting (e.g., Cohen and O'Nions, 1993; Zou and Zindler, 2000). Unfortunately, the Hainan Holocene lavas are about 9000 years (9 ka) old, and thus are too old for the preservation of (^{226}Ra/^{230}Th) disequilibrium, as the half-life of ^{226}Ra is only 1.6 ka.

Nevertheless, the (^{230}Th/^{238}U) disequilibrium alone can place robust constraint on melting rate when the disequilibrium is significant, which is the case for the Hainan Holocene lavas. The explicit relationship between the melting rate and the observed extent of (^{230}Th/^{238}U) disequilibrium (Eq. 3 in Zou et al., 2003) is

$$\dot{M} = \frac{(\lambda_{238} + \lambda_{230})[\rho_f\varphi + \rho_s(1-\varphi)D_U] - Z\lambda_{230}[\rho_f\varphi + \rho_s(1-\varphi)D_{Th}]}{(Z-1)[1 + \rho_f\varphi / [\rho_s(1-\varphi)]]} \quad (4)$$

where Z represents measured (^{230}Th/^{238}U) activity ratios, ϕ is the melting volume porosity, $\dot{M}$ is the melting rate, ρ_f and ρ_s represent the density of melt (2800 g/cm^3) and solid (3300 g/cm^3), respectively. Using the above relationship, Fig. 6 is made to show a plot of melting porosity against melting rate for (^{230}Th/^{238}U) ranging from 1.18 to 1.32. The maximum (^{230}Th/^{238}U) value in the Hainan basalts of 1.32 can be achieved at slow melting rate (<1.0E−4 kg/m^3/year) and low porosity (<0.4%) (Fig. 6). In a one-dimensional melting column, the solid mantle upwelling rate (W) is related to the melting rate ($\dot{M}$), melt productivity (df/dz), and the density of the solid (ρ_s) by $W = \frac{\dot{M}}{\rho_s(df/dz)}$ (Spiegelman and Kenyon, 1992). If the melt productivity df/dz = 0.003 km^{-1} (McKenzie and Bickle, 1988) and density ρ_s = 3300 kg/cm^3 are used, then for melting rate of <1.0E−4 kg/m^3/year, the mantle upwelling rate is <1 cm/year. This indicates that the mantle upwelling is very slow in the Hainan. The plume upwelling beneath Hainan is estimated as significantly slower than the solid mantle upwelling rates for tholeiites from Hawaii plume ranging from 10 to 30 cm/year (Sims et al., 1999). If slow upwelling is usually indicative of dying plumes, the Hainan plume upwelling might be slowing down and might be close to exhausting its source region.

4.4. EM2 Dupal anomaly in Hainan Island

The Dupal isotopic anomaly in some oceanic island and ridge basalts and continental basalts is characterized by high ^{208}Pb/^{204}Pb and ^{207}Pb/^{204}Pb ratios (at a given ^{206}Pb/^{204}Pb ratio) and high ^{87}Sr/^{86}Sr ratio, indicating a reservoir with high time-integrated values of Th/U, ^{235}U/Pb, and Rb/Sr (Dupre and Allegre, 1983; Hart, 1984). Since

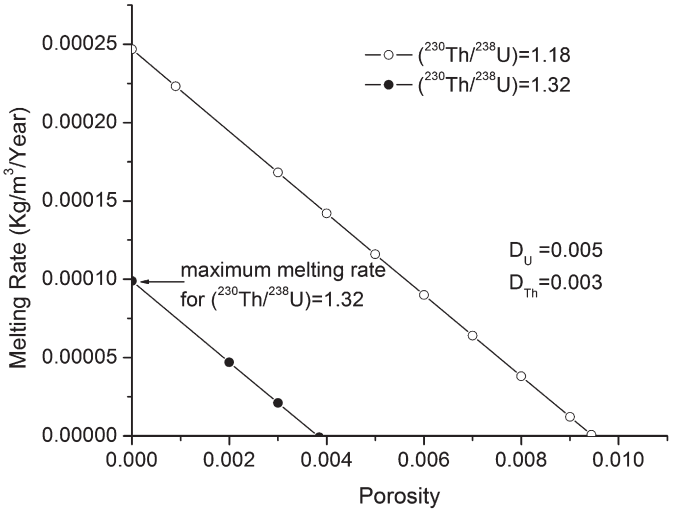

Fig. 6. Estimate of the maximum melting rate from U–Th disequilibrium data. Bulk partition coefficients are $D_U=0.005$ and $D_{Th}=0.003$ for garnet peridotites. Bulk partition coefficients are given by $D_i=\sum K_i x_i$, where K_i is the mineral/melt partition coefficient, and x_i is its mineral proportion in the source. Mineral/melt partition coefficients are: K_{Th}(gt) = 0.019, K_U(gt) = 0.041, K_{Th}(opx) = 0.0002, K_U(opx) = 0.0005 (Salters and Longhi, 1999), K_{Th}(cpx) = 0.015, K_U(cpx) = 0.010 (Lundstrom et al., 1994), and K_{Th}(ol) = K_U(ol) = 0.0001 (assumed). Mineral proportions are: $x_{ol}=61\%$, $x_{opx}=22\%$, $x_{gt}=10\%$, and $x_{cpx}=7\%$. Mineral abbreviations: gt = garnet, opx = orthopyroxene, cpx = clinopyroxene, ol = olivine.

recognition of the Southern Hemisphere Dupal anomaly, its origin remains a geochemical and geophysical enigma. There has been considerable debate about whether Dupal signatures reflect deep or shallow mantle phenomena (Hawkesworth et al., 1986; Castillo, 1988; Sun and McDonough, 1989). The majority of Dupal basalt suites satisfying the requirements of being old, deep and (semi-)global in character clearly occur in the Southern Hemisphere. The South China Sea Basin, including Hainan Island (20ºN), appears to be one of the few Dupal-like domains reported from Northern Hemisphere. The significant ^{230}Th excesses in the young Hainan basalts support for deep mantle reservoirs, instead of local shallow lithospheric mantle origin. If this is also true for older basalts around South China Sea Basin and SE China, then the EM2 domains in South China Sea Basin and SE China may also have deep mantle source.

It has been shown that the source of EM2 ocean island basalts (OIBs) at Samoan islands can be subducted upper continental crust (UCC) materials, owing to the extreme ^{87}Sr/^{86}Sr isotope compositions (0.720469) and negative Nb and Ta anomalies in some Samoan lavas (Jackson et al., 2007). The EM2 Samoan lavas indicate the presence of an ancient recycled UCC component in the Samoan mantle plume and reflect the return of subducted UCC in Samoan lavas (Jackson et al., 2007).

In comparison with the Samoan lavas, the Hainan lavas have not-so-high ^{87}Sr/^{86}Sr isotopic compositions (0.7038 to 0.7043) and display positive Nb or Ta anomalies. Thus the UCC component in the Hainan plume, even if present, is most likely to be insignificant.

Our preferred interpretation is that EM2 characters from Hainan basalts reflect the inherent signatures of the upwelling lower mantle materials. Another possibility is that the source of EM2 from Hainan basalts may have been delaminanted continental (Hainan or south China) lithospheric mantle. The delaminated pieces sank deeper in the mantle where they melted in the seismically anomalous region, and then the melt mixed with depleted material.

The northern boundary of this deep EM2 Dupal source probably extends to SE China basalts with EM2 characters in Fujian and Guangdong provinces (Zou et al., 2000). In contrast, the basalts from NE China, including potassic basalts from Wudalianchi and Jingbohu, show EM1 characters (Basu et al., 1991; Zhang et al., 1991). The EM1 Dupal Pb isotope signatures in these NE China basalts may have originated from the local thick lithosphere beneath NE China.

4.5. The ages of the Pre-Holocene lavas

Our U-series data of older samples provide information on their ages. Note that the U/Th ratio in HN14 is identical to the olivine tholeiites in Maanling (Fig. 6). Assuming the olivine tholeiite from Sanjiaoyuan (HN14) had initial (^{230}Th/^{238}U) ratio at eruption within the range (1.18 to 1.20) of the olivine tholeiites from Maanling, the eruption age of HN14 is 65,000 years (ka) to 77 ka. This 65–77 ka eruption age of HN14 is within the K-Ar age range (60 to 110 ka) (Fan et al., 2004) of the Late Pleistocene volcanic rocks (Daotang Formation) at Hainan.

The quartz tholeiite from Bopian (HN119) displays U–Th equilibrium, suggesting that the age of the older quartz tholeiite is equal to or greater than 375 ka (the five half lives of ^{230}Th). Since quartz tholeiites at Hainan are restricted to the earliest eruptions at Hainan Island (Flower et al., 1992), their secular U–Th equilibrium in HN119 confirms their old age and provided the minimum eruption age (375 ka) for quartz tholeiites. The quartz tholeiites are not Late Pleistocene (10 to 130 ka) volcanic rocks, but may be the Middle to Early Pleistocene or earlier volcanic rocks.

5. Conclusions

1) The Holocene lavas from Maanling and Leihuling volcanoes display strong ^{230}Th excesses (18 to 32%). Their ε_{Nd} values are +4.5 to +4.8 for Maanling lavas, and +4.1 to +4.5 for the Leihuling lavas. All the Hainan lavas show LREE enriched patterns and positive Nb and Ta anomalies.
2) The EM2-like isotopic characteristics in the Hainan basalts were not generated by melting of or contamination by the subcontinental lithosphere. The U–Th disequilibrium data and Nd isotopic compositions support for a model of deep (sub-asthenospheric) melting in the transition zone or more likely the lower mantle (plume melting). It is likely that EM2 component from Hainan basalts represents the isotopic signature of lower mantle component.
3) The upwelling of the Hainan plume is slow (<1 cm/year), which might indicate that Hainan plume is a dying plume that is close to exhausting its source region. Deep melting in the transition zone or lower mantle generates the Hainan Island basalts with Dupal-like EM2 Pb isotope signatures. The older EM2 Cenozoic basalts from South China Sea Basin and in SE China areas might also have been derived from decompressional melting of lower mantle materials associated with the rising Hainan plume.

Acknowledgements

We are grateful to Asish R. Basu, Pat Castillo, and Andrew C. Kerr for their constructive reviews that significantly improved the quality of this paper. We thank Kevin McKeegan, Mary Reid, Axel K. Schmitt, and Xisheng Xu for their help, Qian Sun and Jianli Sui for field assistance, and Dapeng Zhao for fruitful discussion. Andrew C. Kerr provided speedy handling of the manuscript. This work has been supported by National Science Foundation (NSF EAR 0917651) and Chinese National Science Foundation (40972047). The ion microprobe facility at UCLA is partly supported by a grant from the Instrumentation and Facilities Program, Division of Earth Sciences, NSF.

References

Asmerom, Y., 1999. Th–U fractionation and mantle structure. Earth and Planetary Science Letters 166, 163–175.
Asmerom, Y., Edwards, R.L., 1995. U-series isotope evidence for the origin of continental basalts. Earth and Planetary Science Letters 134, 1–7.
Basu, A.R., Wang, J.W., Huang, W.K., Xie, G.H., Tatsumoto, M., 1991. Major element, REE, and Pb, Nd and Sr isotopic geochemistry of Cenozoic volcanic rocks of eastern China: implications for their origin from suboceanic-type mantle reservoirs. Earth and Planetary Science Letters 105, 149–169.
Beattie, P., 1993. Uranium–thorium disequilibria and partitioning on melting of garnet peridotite. Nature 363, 63–65.
Castillo, P., 1988. The Dupal anomaly as a trace of the upwelling lower mantle. Nature 336, 667–670.
Chabaux, F., Allegre, C.J., 1994. ^{238}U–^{230}Th–^{226}Ra disequilibria in volcanics: a new insight into melting conditions. Earth and Planetary Science Letters 126, 61–74.
Cohen, A.S., O'Nions, R.K., 1993. Melting rates beneath Hawaii: evidence from uranium series isotopes in recent lavas. Earth and Planetary Science Letters 120, 169–175.
Dupre, B., Allegre, C.J., 1983. Pb–Sr isotope variation in Indian Ocean basalts and mixing phenomena. Nature 303, 142–146.
Elliott, T., 2003. Tracers of the slab. In: Eiler, J. (Ed.), Inside the Subduction Factory. Geophysical Monograph, vol. 138. American Geophysical Union, pp. 23–45.
Elliott, T., Plank, T., Zindler, A., White, W., Bourdon, B., 1997. Elemental transport from slab to volcanic front at the Mariana arc. Journal of Geophysical Research 102, 14,991–15,019.
Fan, Q.C., Sun, Q., Li, N., Sui, J.L., 2004. Periods of volcanic activity and magma evolution during Holocene in the northern Hainan Island. Acta Petrologica Sinica 20, 533–544.
Flower, M.F., Zhang, M., Chen, C.Y., Tu, K., Xie, G.H., 1992. Magmatism in the South China Basin 2. Post-spreading Quaternary basalts from Hainan Island, south China. Chemical Geology 97, 65–87.
Frey, F.A., Green, D.H., Roy, S.D., 1978. Integrated models of basalts petrogenesis: a study of quartz tholeiite to olivine melilitites from South Eastern Australia utilizing geochemical and experimental data. Journal of Petrology 19, 463–513.
Gill, J.B., 1981. Orogenic Andesites and Plate Tectonics. Springer-Verlag, Beilin. 330 pp.
Gill, J.B., Williams, R.W., 1990. Th isotope and U-series studies of subduction-related volcanic rocks. Geochmica et Cosmochimica Acta 54, 1427–1442.
Hart, S.R., 1984. A large-scale isotope anomaly in the Southern Hemisphere mantle. Nature 309, 753–757.
Hart, S.R., Hauri, E.H., Oschmann, L.A., Whitehead, J.A., 1992. Mantle plumes and entrainment — isotopic evidence. Science 256, 517–520.

Hawkesworth, C.J., Mantovani, M.S.M., Taylor, P.N., Palacz, Z., 1986. Evidence from the Parani of south Brazil for a continental contribution to Dupal basalts. Nature 322, 356–358.
Hawkesworth, C.J., Kempton, P.D., Rogers, N.W., El-lain, R.W., van Calsteren, P.W., 1990. Continental mantle lithosphere and shallow level enrichment processes in the Earth's mantle. Earth and Planetary Science Letters 96, 256–268.
Hirschmann, M.M., Kogiso, T., Baker, M.B., Stolper, E.M., 2003. Alkalic magmas generated by partial melting of garnet pyroxenite. Geology 31, 481–484.
Hoang, N., Flower, M., 1998. Petrogenesis of Cenozoic basalts from Vietnam: implication for origins of a 'Diffuse Igneous Province'. Journal of Petrology 39, 369–395.
Huang, J.L., Zhao, D.P., 2006. High-resolution mantle tomography of China and surrounding regions. Journal of Geophysical Research 111, B09305. doi:10.1029/2005JB004066.
Jackson, M.G., Hart, S.R., Koppers, A.A.P., Staudigel, H., Konter, J., Blusztajn, J., Kurz, M., Russell, J.A., 2007. The return of subducted continental crust in Somoan lavas. Nature 448, 684–687.
Kogiso, T., Hirschmann, M.M., Frost, D.J., 2003. High-pressure partial melting of garnet pyroxenite: possible mafic lithologies in the source of ocean island basalts. Earth and Planetary Science Letters 216, 603–617.
LaTourrette, T.Z., Kennedy, A.K., Wasserburg, G.J., 1993. Thorium–uranium fractionation by garnet: evidence for a deep source and rapid rise of oceanic basalts. Science 261, 739–742.
Lebedev, S., Nolet, G., 2003. Upper mantle beneath Southeast Asia from S velocity tomography. Journal of Geophysical Research 108, 2048. doi:10.1029/2000JB000073.
Leeman, W.P., Schutt, D.L., Hughes, S.S., 2009. Thermal structure beneath the Snake River Plain: implication for the Yellowstone hotspot. Journal of Volcanology and Geothermal Research 188, 57–67.
Lei, J.S., Zhao, D.P., 2009. New seismic constraints on the upper mantle structure of the Hainan plume. Physics of the Earth and Planetary Interiors 173, 33–50.
Liu, J.Q., 1999. Chinese Volcanoes. Scientific Publishing. 219 pp.
Lundstrom, C.C., Shaw, H.F., J., R.F., L., P.D., G.J., B., Q., W., 1994. Compositional controls on the partitioning of U, Th, Ba, Pb, Sr, and Zr between clinopyroxene and haplobasaltic melts: implications for uranium series disequilibria in basalts. Earth and Planetary Science Letters 128, 407–423.
Mahoney, J.J., Natland, J.H., White, W.M., Poreda, R., Bloomer, S.H., Fisher, R.L., Baxter, A. N., 1989. Isotopic and geochemical provinces of the western Indian Ocean spreading. Journal of Geophysical Research 94, 4033–4052.
Manea, V.C., Manea, M., Leeman, W.P., Schutt, D.L., 2009. The influence of plume head-lithosphere interaction on magmatism associated with the Yellowstone hotspot track. Journal of Volcanology and Geothermal Research 188, 68–85.
McKenzie, D., Bickle, M.J., 1988. The volume and composition of melt generated by extension of the lithosphere. Journal of Petrology 29, 625–679.
Pietruszka, A.J., Rubin, K.H., Garcia, M.O., 2001. ^{226}Ra–^{230}Th–^{238}U disequilibria of historic Kilauea lavas (1790–1982) and the dynamics of mantle melting within the Hawaiian plume. Earth and Planetary Science Letters 186, 15–31.
Reid, M.R., 1995. Processes of mantle enrichment and magmatic differentiation in the eastern Snake River Plain: Th isotope evidence. Earth and Planetary Science Letters 131, 239–254.
Salters, V.J.M., Longhi, J., 1999. Trace element partitioning during the initial stages of melting beneath mid-ocean ridges. Earth and Planetary Science Letters 166, 15–30.
Sims, K.W.W., DePaolo, D.J., Murrell, M.T., Baldredge, W.S., Goldstein, S., Clague, D., Jull, M., 1999. Porosity of the melting zone and variations in the solid mantle upwelling rate beneath Hawaii: inferences from ^{238}U–^{230}Th–^{226}Ra and ^{235}U–^{231}Pa disequilibria. Geochimica et Cosmochimica Acta 63, 4119–4138.
Spiegelman, M., Kenyon, P., 1992. The requirements for chemical disequilibrium during magma migration. Earth and Planetary Science Letters 109, 611–620.
Sun, S.S., McDonough, W.F., 1989. Chemical and isotopic systematics of oceanic basalts: implications for mantle composition and processes. In: Saunders, A.D., Norry, M.J. (Eds.), Magmatism in the Ocean Basins: Geological Society Special Publication, London, pp. 313–345.
Todt, W., Cliff, R.A., Hanser, A., Hofmann, A.W., 1996. Evaluation of a ^{202}Pb–^{205}Pb double spike for high-precision lead isotope analysis. In: Basu, A.R., Hart, S.R. (Eds.), Earth Processes: Reading the Isotopic Code: Geophysical Monograph Am. Geophys. Union, pp. 429–437.
Tu, K., Flower, M.F.J., Carlson, R.W., Zhang, M., Xie, G., 1991. Sr, Nd, and Pb isotopic compositions of Hainan basalts (south China): implications for a subcontinental lithosphere Dupal source. Geology 19, 567–569.
Tu, K., Flower, M.F.J., Carlson, R.W., Xie, G.H., Chen, C.Y., Zhang, M., 1992. Magmatism in the South China Basin, 1. Isotopic and trace element evidence for an endogenous Dupal mantle component. Chemical Geology 97, 47–63.
Turner, S.P., Bourdon, B., Gill, J.B., 2003. Insights into magma genesis at convergent margins from U-series isotopes. In: Bourdon, B., Henderson, G.M., Lundstrom, C.C., Turner, S.P. (Eds.), Uranium-series Geochemistry: Reviews in Mineralogy and Geochemistry, pp. 255–310.
Williams, R.W., Gill, J.B., 1989. Effect of partial melting on the uranium decay series. Geochimica et Cosmochimica Acta 53, 1607–1619.
Wu, H.H., Tsai, Y.B., Lee, T.Y., Lo, C.H., H, H.C., Toan, D.V., 2004. 3-D shear wave velocity structure of the crust and upper mantle in South China Sea and its surrounding regions by surface wave dispersion analysis. Marine Geophysical Research 25, 5–27.
Zhang, M., Menzies, M.A., Suddaby, P., Thirlwall, M.F., 1991. EM1 signature from the post-Archaean subcontinental lithospheric mantle: isotopic evidence from the potassic volcanic rocks in NE China. Geochemical Journal 25, 387–398.
Zhao, D.P., 2004. Global tomographic images of mantle plumes and subducting slabs: insight into deep Earth dynamics. Physics of the Earth and Planetary Interiors 146, 3–34.
Zhao, D.P., 2007. Seismic images under 60 hotspots: search for mantle plumes. Gondwana Research 12, 335–355.
Zhou, P.B., Mukasa, S.B., 1997. Nd–Sr–Pb isotopic, and major- and trace-element geochemistry of Cenozoic lavas from the Khorat Plateau, Thailand: source and petrogenesis. Chemical Geology 137, 175–193.
Zindler, A., Hart, S.R., 1986. Chemical geodynamics. Annual Review of Earth Planetary Sciences 14, 493–571.
Zou, H.B., 1998. Trace element fractionation during modal and nonmodal dynamic melting and open-system melting: a mathematical treatment. Geochimica et Cosmochimica Acta 62, 1937–1945.
Zou, H.B., Zindler, A., 1996. Constraints on the degree of dynamic partial melting and source composition using concentration ratios in magmas. Geochimica et Cosmochimica Acta 60, 711–717.
Zou, H.B., Zindler, A., 2000. Theoretical studies of ^{238}U–^{230}Th–^{226}Ra and ^{231}Pa–^{235}U disequilibria in young lavas produced during mantle melting. Geochimica et Cosmochimica Acta 64, 1809–1817.
Zou, H.B., Zindler, A., Xu, X.S., Qi, Q., 2000. Major and trace element, and Nd–Sr–Pb isotope studies of Cenozoic basalts in SE China: mantle sources, regional variations, and tectonic significance. Chemical Geology 171, 33–47.
Zou, H.B., Reid, M.R., Liu, Y.S., Yao, Y.P., Xu, X.S., Fan, Q.C., 2003. Constraints on the origin of historic potassic basalts from northeast China by U–Th disequilibrium data. Chemical Geology 200, 189–201.
Zou, H.B., Fan, Q.C., Yao, Y.P., 2008. U–Th systematics of dispersed young volcanoes in NE China: asthenosphere upwelling caused by piling up and upward thickening of stagnant Pacific slab. Chemical Geology 255, 134–142.